



# Surface thermal stability of iron pyrite nanocrystals: Role of capping ligands



Baodong Mao<sup>a</sup>, Qingfeng Dong<sup>a</sup>, Christopher L. Exstrom<sup>b</sup>, Jinsong Huang<sup>a,\*</sup>

<sup>a</sup> Department of Mechanical and Materials Engineering, University of Nebraska-Lincoln, Lincoln, NE68588, United States

<sup>b</sup> Department of Chemistry, University of Nebraska-Kearney, Kearney, NE68849, United States

## ARTICLE INFO

### Article history:

Received 7 October 2013

Received in revised form 5 April 2014

Accepted 9 April 2014

Available online 18 April 2014

### Keywords:

Iron pyrite  
FeS<sub>2</sub> nanocrystals  
Thin films  
Ligand exchange  
Surface stability  
Photovoltaic

## ABSTRACT

Iron pyrite (FeS<sub>2</sub>) is a promising photovoltaic absorber material with a high natural abundance and low cost, but surface defects and low photoresponse inhibit sunlight energy conversion. The surface stability of pyrite FeS<sub>2</sub> nanocrystals synthesized in oleylamine (OLA) with trioctylphosphine oxide (TOPO) as an additional capping ligand was investigated using Fourier transform infrared spectroscopy, Raman spectroscopy and X-ray diffraction. Tunable laser exposure during Raman spectroscopy measurement was developed for convenient and systematic evaluation of the stability of FeS<sub>2</sub> nanocrystals. The surface stability of 100–200 nm diameter cubic nanocrystals with long-chain (OLA, TOPO) or small-molecule (pyridine) capping ligands was evaluated after high-intensity laser exposure as well as after thermal annealing in air and N<sub>2</sub>. While increasing surface coverage with OLA and TOPO capping ligands provided additional protection against oxidation, FeS<sub>2</sub> nanocrystals capped with pyridine showed good stability at temperatures up to 200 °C in air and 400 °C in N<sub>2</sub>. These results provide greater understanding of the processing of nanocrystal-based iron pyrite thin films for photovoltaic applications.

© 2014 Elsevier B.V. All rights reserved.

## 1. Introduction

Due to its high natural abundance, nontoxicity, low cost and the high absorption coefficient of  $1\text{--}5 \times 10^5 \text{ cm}^{-1}$  [1,2], an attractive application of iron pyrite (FeS<sub>2</sub>) is as a photovoltaic (PV) absorber material. The estimated highest attainable efficiency of pyrite PV energy conversion is as high as that of single crystal silicon solar cells [3]. This prospectus is further promoted with the recent development of highly crystalline, phase-pure iron pyrite nanocrystal (NC) inks that enable large throughput and low cost fabrication of solar panels using established solution-based techniques [4–11]. Despite the huge promise iron pyrite holds, this material has not yet been developed into efficient PV devices. The highest pyrite PV device efficiency has been obtained in a photoelectrochemical cell with a reported short circuit current ( $I_{sc}$ ) of 42 mA/cm<sup>2</sup>, open circuit voltage ( $V_{oc}$ ) of 187 mV, and fill factor ( $FF$ ) of 50%, yielding an efficiency of 2.8% [2,12]. The limiting factor for high efficiency is the high dark current that leads to the very small  $V_{oc}$ , less than 20% of its bandgap (0.95 eV) [2,12–16].

Natural bulk pyrite and synthetic thin films generally have common traits of high carrier concentrations in excess of  $10^{19} \text{ cm}^{-3}$  and strong sub-bandgap absorption [17–19]. Photoresponse (e.g., photoconductivity) of these grown films has barely been observed at room temperature [20,21]. There are two types of possible factors that lead to the high dark carrier concentrations in iron pyrite: impurity phases and surface

defects. Previously it was believed that impurity phases such as marcasite and hexagonal troilite have much smaller bandgaps (0.34 eV for marcasite and 0.04 eV for troilite) [22]. More recently Law et al. declared that marcasite had band gap comparable to pyrite [23]. They also suggested that the high conductivity and low mobility of pyrite films might be caused by nanoscale amorphous impurities and surface effect and excluded the intrinsic bulk defects [23]. The surfaces of iron pyrite are terminated with S dimmers, that tend to segregate to the surface and cause the vanishing of the hybridized band at the top of the Fe layer, making the surface effectively similar to 1S terminated troilite or FeS<sub>2-x</sub>. This results in large density-of-defect states in the middle of pyrite bandgap that reduced the bandgap energy at the surface to nearly zero [5,24]. Pyrite films may be heavily hole doped due to a hole-rich layer formed at the surface resulted from a large concentration of surface states located near the valence band edge and even in pyrite single crystals there might exist an n-type bulk layer and a p-type surface layer according to recent experimental work [23]. Although not conclusive, more and more evidence shows that the surface defects dominate the generation of large density of background charge density. It is suggested by theoretical calculations that FeS<sub>2</sub> is actually a stoichiometric compound because of the high energy required to generate S vacancies in bulk FeS<sub>2</sub>, and thus, bulk defects are unlikely to cause the large carrier concentrations [19]. Instead of bulk S vacancies, the presence of high-density S vacancies at the surface has been calculated to be favorable in CoS<sub>2</sub> which has the same structure with FeS<sub>2</sub> [25,26]. Recent high resolution transmission electron microscopy studies of sulfurized pyrite films clearly revealed a S-deficient amorphous surface

\* Corresponding author. Tel.: +1 402 472 2640; fax: +1 402 472 1465.  
E-mail address: [jhuang2@unl.edu](mailto:jhuang2@unl.edu) (J. Huang).

despite annealing in a very S-rich environment [19]. The pyrite crystal surfaces suffer incomplete coordination of iron by S due to the loss of S from the surface [27].

Using iron pyrite NCs to fabricate the photovoltaic films avoids the formation of impurity phases as proven by their excellent phase purity and crystallinity [4,5,22,28]. However, the significantly larger surface-to-volume ratio of NCs is expected to bring challenges in maintaining stable iron pyrite surfaces. To our surprise, NC-based FeS<sub>2</sub> films show better stability than those made by other methods as indicated by the observed room temperature photoresponse in iron pyrite films [5]. The surface capping ligands on these NCs are proposed to play the major role in stabilizing the NC surface. Introducing surfactant capping ligands to stabilize NC surfaces is a commonly employed strategy in NC synthesis. The situation is especially complex for FeS<sub>2</sub> NCs because in addition to size and shape, the crystallinity and phase purity [22], colloidal stability against aggregation [29,30], stability of NC films [5], and optoelectronic properties [5,31,32], all have showed strong dependence on the surfactants used during NC synthesis or post-treatment.

In this paper, the function of ligands in stabilizing FeS<sub>2</sub> NC surface was studied by monitoring the thermal stability of FeS<sub>2</sub> NCs in air and N<sub>2</sub> after removing long alkane ligands by solvent wash, or exchanging the long ligand with short ligands of pyridine. The role of ligands in the oxidization behavior of FeS<sub>2</sub> NCs capped with different length ligands upon high-intensity laser irradiation and thermal annealing was investigated systematically using Raman spectroscopy and X-ray diffraction (XRD). Efforts were focused on determining the importance of the nature of the capping ligands, how they protect the thin films, and how these issues impact future device fabrication and processing.

## 2. Experimental details

### 2.1. Synthesis of FeS<sub>2</sub> NCs

Anhydrous iron (II) chloride (99.9%), sulfur (98%), trioctylphosphine oxide (TOPO), oleylamine (OLA), chloroform and methanol were purchased from Sigma-Aldrich. All chemicals were used as received without further purification. Cubic shaped FeS<sub>2</sub> NCs were synthesized by the hot injection method reported previously with minor modifications [5]. In brief, a mixture containing 0.5 mmol of FeCl<sub>2</sub>, 0.3 mmol of TOPO and 10 ml of OLA was heated to 170 °C and kept at that temperature for 2 h under N<sub>2</sub> to form Fe-surfactant precursor species. A solution of 3 mmol sulfur in 5 ml OLA was injected quickly into the Fe precursor and then the system was immediately heated to 220 °C and kept at that temperature for 2 h to complete the growth of the iron pyrite NCs. The reaction was terminated by removing the heating mantle and cooled down to room temperature naturally.

The FeS<sub>2</sub> NCs were precipitated by adding excess methanol and isolated by centrifugation at 3000 rpm for 10 min. For selected experiments, these as-prepared NCs were washed with chloroform/methanol, sonicated, and isolated by centrifugation to remove the excess of OLA and TOPO. These NCs were denoted as FeS<sub>2</sub>-OLA/TOPO. To prepare pyridine-capped FeS<sub>2</sub> NCs (denoted as FeS<sub>2</sub>-pyridine), the FeS<sub>2</sub>-OLA/TOPO NCs were dispersed in 10 ml of pyridine, sonicated for 10 min and isolated by centrifugation. This process was repeated one more time to ensure the maximum exchange of the long-chain OLA and TOPO ligands by pyridine. Pyridine was chosen for ligand exchange because pyridine capped NCs are still dispersible in organic solvents, which are superior to ethanedithiol that causes aggregation of NCs and can only be applied for post-treatment of NC films. Both FeS<sub>2</sub>-OLA/TOPO and FeS<sub>2</sub>-pyridine NC samples were dispersed in chloroform and kept in a N<sub>2</sub> filled glove box for storage prior to further characterization.

NC-based thin films were formed on 1 × 1 cm<sup>2</sup> silicon wafers by drop casting from FeS<sub>2</sub> NC/chloroform dispersions. These films were annealed on a hot plate in air or in N<sub>2</sub> at different temperatures for 20 min, respectively. All of these FeS<sub>2</sub> films were stored in a N<sub>2</sub> filled glove box before

XRD and Raman measurements to avoid the unintentional gradual oxidation or decomposition of the FeS<sub>2</sub> NCs in air.

### 2.2. Characterization

The presence and exchange of capping ligands on FeS<sub>2</sub> NCs were identified by Fourier transform infrared spectra (FTIR) using a Nicolet Avatar spectrometer. A drop of the FeS<sub>2</sub> NC/chloroform dispersion was mixed with dry KBr powder (FT-IR grade, Alrich), and the solvent was allowed to evaporate. This mixture was ground and pressed into pellets for FTIR measurements. Morphology and size of the NCs were characterized by scanning electron microscopy (SEM) using a Quanta 200 FEG SEM at high vacuum mode with the operating voltage of 15 kV. The thermal stability of FeS<sub>2</sub> samples was investigated by Confocal Raman spectroscopy (RenishawinVia) with a 514 nm laser source. To investigate the effect of light intensity on the oxidation of the FeS<sub>2</sub> NCs, lasers with power of 1.5, 7.5 and 15 mW were focused on sample spots of approximately 25 μm<sup>2</sup> with the irradiation time of 10 s. These laser powers corresponded to power intensities of 6.0 × 10<sup>6</sup>, 3.0 × 10<sup>7</sup> and 6.0 × 10<sup>7</sup> mW/cm<sup>2</sup>, respectively. The laser penetration depth is ~60 nm estimated by 1/α, where α is the absorption coefficient (~1.7 × 10<sup>5</sup> cm<sup>-1</sup> at 514 nm) of the FeS<sub>2</sub> NCs [5,33]. Powder X-ray diffraction (XRD) patterns of the FeS<sub>2</sub> NC films were collected on a Rigaku D/Max-B diffractometer with Bragg–Brentano parafocusing geometry (Co Kα, λ = 1.7902 Å) with X-ray tube operating voltage of 40 kV and current of 30 mA.

## 3. Results and discussion

### 3.1. Ligand exchange studies

SEM images of the as-prepared pyrite FeS<sub>2</sub> NCs show that they had cubic shapes and diameters ranging between 100 and 200 nm (Fig. 1b). FTIR spectroscopy was used to identify the presence of OLA and TOPO capping ligands on the FeS<sub>2</sub> NCs (Fig. 1a). FTIR spectra of pure OLA and TOPO are also shown for comparison. The IR spectrum of OLA shows peaks at 2921 and 2852 cm<sup>-1</sup> that correspond to the asymmetric (ν<sub>2</sub>(-CH<sub>2</sub>-)) and symmetric (ν<sub>3</sub>(-CH<sub>2</sub>-)) stretching modes, respectively, of the oleyl groups. The peak at 3315 cm<sup>-1</sup> is due to the ν(N-H) stretching of the -NH<sub>2</sub> group. There is a small peak at approximately 1650 cm<sup>-1</sup> due to ν(C=C) stretching in OLA molecules [34]. The peaks in the region below 1650 cm<sup>-1</sup> correspond to complex combinations of the ν(C-C) stretching, CH<sub>2</sub> deformations and other motions [34]. All of these OLA peaks were seen in the FeS<sub>2</sub>-OLA/TOPO NC spectrum (Fig. 1a, green curve) indicating the existence of this long-chain ligand on the NCs after washing.

For TOPO, there are also two peaks around 2900 cm<sup>-1</sup> assigned to the stretching mode of -CH<sub>2</sub> in the octyl group. Characteristic vibration bands of P=O and P-C groups in TOPO are observed at 1149 cm<sup>-1</sup> and 1411 cm<sup>-1</sup>, respectively. The IR spectrum of the FeS<sub>2</sub>-OLA/TOPO NCs clearly shows peaks that indicate the presence of OLA. While many of the TOPO P=O and P-C vibrational frequencies match those of OLA peaks, the presence of at least a small amount of TOPO is indicated in the 650–1250 cm<sup>-1</sup> region of the spectrum. This evidence indicates that OLA and TOPO capping ligands are present on the FeS<sub>2</sub> NCs after three washing cycles with chloroform/methanol. After ligand exchange with pyridine, the FeS<sub>2</sub>-pyridine NC IR spectrum (blue curve in Fig. 1a) exhibits very little signal from OLA and TOPO, indicating the removal of most of the long-chain ligands.

### 3.2. Stability study of the FeS<sub>2</sub> NCs by Raman spectroscopy

#### 3.2.1. Thermal stability of FeS<sub>2</sub>-OLA/TOPO NCs

Raman spectroscopy was employed to investigate the thermal stability and surface chemistry of the FeS<sub>2</sub> NC samples. Fig. 2 shows Raman spectra of FeS<sub>2</sub>-OLA/TOPO NC samples after exposure to various

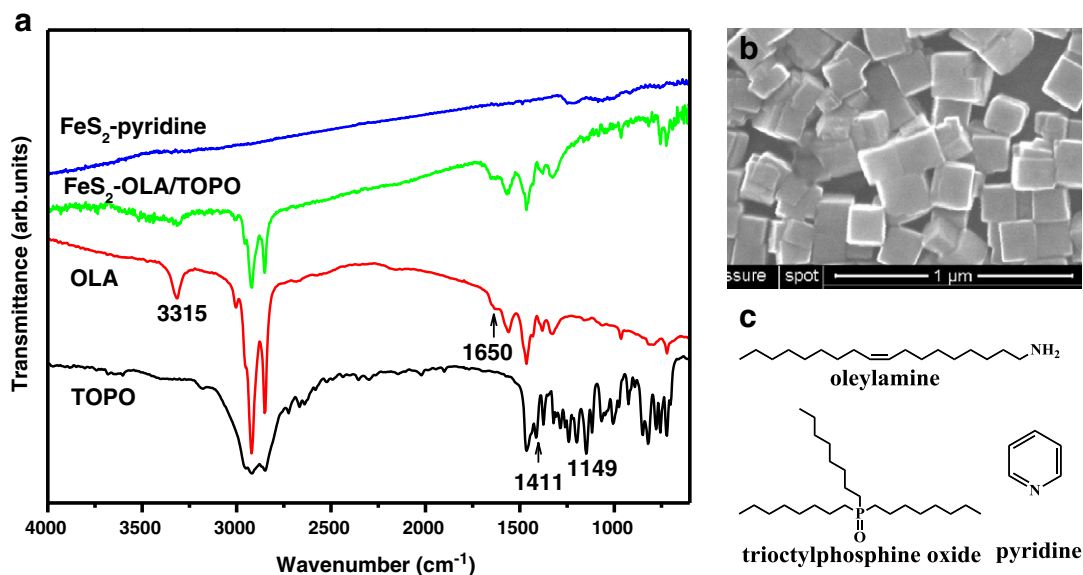


**Fig. 1.** (a) FTIR spectra of TOPO, OLA, as-prepared FeS<sub>2</sub>-OLA/TOPO NCs, and FeS<sub>2</sub>-pyridine NCs after ligand exchange. (b) SEM images of the cubic shaped FeS<sub>2</sub> NCs. (c) Chemical structures of the capping ligands used.

laser power levels. After 1.5 mW laser exposure, the sample maintained the pure iron pyrite phase. The 338 and 371 cm<sup>-1</sup> peaks are assigned to the E<sub>g</sub> and A<sub>g</sub> modes, respectively, of pyrite-phase FeS<sub>2</sub>. Following exposure to 5 times higher power laser (7.5 mW) gave stronger Raman signals while did not result in the formation of other noticeable phases (red curve in Fig. 2). Further increase in the laser power to 10 times higher (15 mW), two new peaks at 215 and 278 cm<sup>-1</sup> appeared and are assigned to a lattice mode and the symmetric stretching mode, respectively, of poorly crystallized or nanophase FeS [35–37]. This result indicates that the FeS<sub>2</sub> NCs were partially decomposed. We expect that the surface of the FeS<sub>2</sub> NCs under high power (15 mW) laser had undergone the following rapid decomposition reaction [5,24]:



The laser powers employed,  $6.0 \times 10^6$ ,  $3.0 \times 10^7$  and  $6.0 \times 10^7$  mW/cm<sup>2</sup>, respectively, are far higher than that of AM1.5 simulated sunlight (100 mW/cm<sup>2</sup>). Exposure to this high intensity laser is expected to result

in a significant heat accumulation in the small measured area and subsequently accelerate the surface decomposition of the pyrite NCs. It is noted that laser annealing or high intensity flash light is broadly used to melt preformed NCs for polycrystalline solar cell fabrication, the understanding of stability of the NCs upon laser annealing is thus practically important.

### 3.2.2. Improved surface stability of FeS<sub>2</sub> NCs by long-chain capping ligands

After knowing the effect of laser power on the surface decomposition of the FeS<sub>2</sub> NCs, we continued to use the highest power (15 mW) to investigate their stability after multiple cycles washing to remove capping ligands gradually. As shown in Fig. 3, the thermal stability of FeS<sub>2</sub> samples decreased as the long chain ligands TOPO and OLA were partially removed. FeS<sub>2</sub> NCs easily underwent decomposition after washing three times when the greatest portion of the FeS<sub>2</sub> NC surface was exposed to strong laser irradiation in air. The observed improved stability by these capping ligands demonstrates the important role of the TOPO and OLA ligands against decomposition of the FeS<sub>2</sub> NCs.

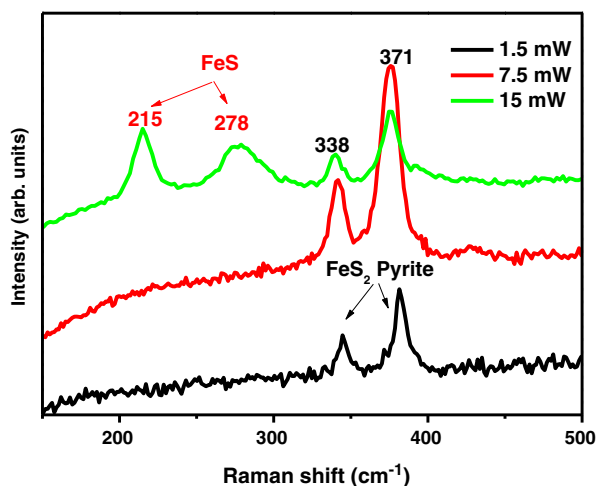


**Fig. 2.** Raman spectra of the as-prepared FeS<sub>2</sub>-OLA/TOPO NCs after exposure to laser power of 1.5 (black), 7.5 (red) and 15 mW (green), approximately corresponding to power intensities of  $6.0 \times 10^6$ ,  $3.0 \times 10^7$  and  $6.0 \times 10^7$  mW/cm<sup>2</sup>, respectively.

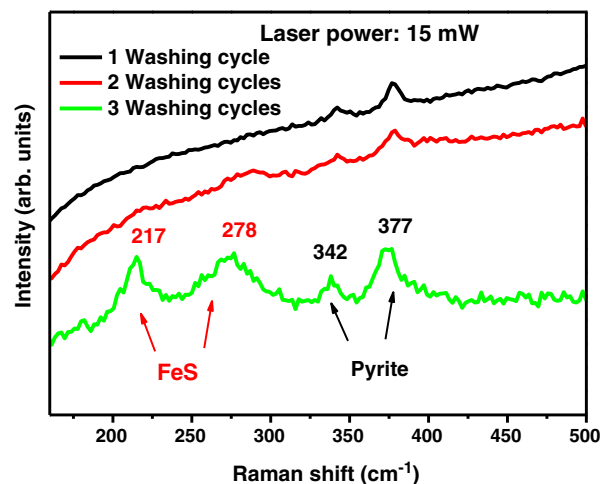


**Fig. 3.** Raman spectra of the as-prepared FeS<sub>2</sub> NCs capped with OLA and TOPO and different degrees of washing with chloroform/methanol after exposure to 15 mW laser.

### 3.2.3. Surface stability of FeS<sub>2</sub> NCs capped with a small-molecule ligand

Ligand exchange with small molecules, such as pyridine and ethanedithiol, to replace longer surfactant ligands such as OLA and TOPO is a commonly employed strategy in fabricating NC devices to enhance the electronic coupling between NCs [32]. The effect of short chain (pyridine) and long chain (OLA:TOPO) capping ligands on the stability was investigated by Raman spectroscopy as shown in Fig. 4. Both OLA:TOPO capped and pyridine capped FeS<sub>2</sub> NC films were found to be stable under the exposure to 1.5 mW laser power. However, under higher laser power of 7.5 mW, the emergence of the 216 and 276 cm<sup>-1</sup> Raman peaks of FeS indicates that the pyridine FeS<sub>2</sub> NCs were partially decomposed (blue curve), while the OLA:TOPO capped FeS<sub>2</sub> NC films did not show noticeable decomposition (green curve). The long chain ligands of OLA and TOPO can more effectively protect the FeS<sub>2</sub> NC surface by forming a closely coordinated shell on the NC surface. Nevertheless, pyridine-capped FeS<sub>2</sub> NCs showed good stability against oxidation upon exposure to 1.5 mW laser power. These NCs are still relatively stable in air under light illumination that is much higher than sunlight.

Teo et al. investigated the structural conversion of FeS and CoSe to pyrite phase FeS<sub>2</sub> and CoSe<sub>2</sub> induced by high energy laser during Raman measurement [33]. Their work demonstrated that controllable laser irradiation is an effective method for in situ investigation of phase change of metal chalcogenide thin films or powders and gives instructive information on how to avoid laser-induced structural changes and oxidation of metal chalcogenide materials (without surface ligand protection). The situation is more complex in FeS<sub>2</sub> NCs considering the small size and high surface-to-volume ratio, where surface protection of the NCs played a key role. In the present work, we used iron pyrite NCs capped with different kinds of ligands and investigated the roles of laser power, surface coverage of the NCs, and chain length of the capping ligands in the effective protection of the iron pyrite NCs. The maximum laser intensity in the present work (6.0 × 10<sup>7</sup> mW/cm<sup>2</sup>) is coincidentally the same with that used in Teo's work [33]. The effect of ligand protection against decomposition is observed upon different laser intensities and the FeS<sub>2</sub> NCs show good stability with lower laser intensities even without long chain ligand protection.

### 3.2.4. Thermal stability of FeS<sub>2</sub> NCs in air and in N<sub>2</sub>

In addition, we also used Raman spectroscopy to investigate the oxidation process of thermally annealed FeS<sub>2</sub> NCs in N<sub>2</sub> and air

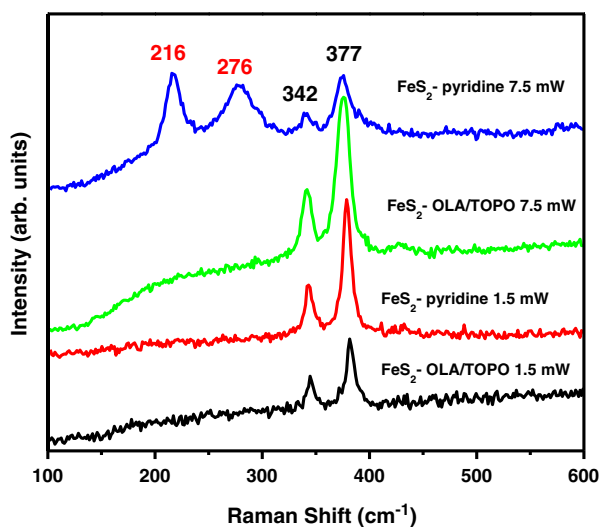


Fig. 4. Raman spectra of FeS<sub>2</sub>-OLA/TOPO and FeS<sub>2</sub>-pyridine NC films exposed to 1.5 mW and 7.5 mW laser power.

atmospheres. A laser power of 1.5 mW was chosen to avoid additional reactions caused by laser heating during Raman measurements. As shown in Fig. 5, Raman spectra of the TOPO:OLA-capped FeS<sub>2</sub> NCs did not show any noticeable change after annealing in N<sub>2</sub> at 400 °C. Annealing in air at 200 °C for 20 min also did not result in noticeable oxidation. This lends promise to the idea of oxygen doping of pyrite that has been proposed to increase its bandgap for improved PV performance [38]. A controllable oxygen doping may be achieved by mild air annealing of NCs with proper ligand protection. The capping ligands could be removed after annealing. After heating at 400 °C in air for 20 min, the 224, 289 and 410 cm<sup>-1</sup> (Fig. 5, cyan curve) can be indexed to α-Fe<sub>2</sub>O<sub>3</sub> [39] indicating that the FeS<sub>2</sub> NCs were completely oxidized with the disappearance of the pyrite peaks at 342 and 377 cm<sup>-1</sup>. Given the boiling points of OLA (364 °C) and TOPO (411 °C), it is possible that the ligand can be evaporated from the NC surface or decomposed at such a high temperature, leaving exposed iron pyrite NC surfaces to react with air.

### 3.3. Phase change of the thermally treated FeS<sub>2</sub> NCs by XRD

In order to verify the oxidation process of the FeS<sub>2</sub> NCs in air at high temperature, we measured the XRD patterns of FeS<sub>2</sub> NCs with different ligands annealed in air and N<sub>2</sub> with increasing temperature, as shown in Fig. 6. The peaks of FeS<sub>2</sub> NCs without annealing can be indexed to iron pyrite (PDF# 42-130). No noticeable oxidation of the FeS<sub>2</sub> samples was detected by XRD after thermal treatment at 200 °C. In addition, there are several unassigned small peaks in Fig. 6 (denoted by circles) that are possibly due to the air exposure product of the capping ligands (oleylamine), which disappeared with further increase of annealing temperature. After thermal treatment of 20 min at 300 °C in air, both FeS<sub>2</sub>-OLA/TOPO and FeS<sub>2</sub>-pyridine NC films were partially oxidized. Both of the NC films were completely oxidized after thermal treatment at 400 °C in air for 20 min, and the diffraction peaks corresponding to FeS<sub>2</sub> almost disappeared (blue curves in Fig. 6a and b).

Annealing in a N<sub>2</sub> atmosphere from 200 to 400 °C did not result in noticeable phase changes. This was consistent with the Raman spectroscopy studies. The thermal stability against decomposition in an inert atmosphere is similar to previously reported results of bulk FeS<sub>2</sub> that is stable up to 400 °C upon annealing without air [24]. According to the XRD spectra of completely oxidized FeS<sub>2</sub> samples (blue curves, 400 °C), the main oxidation product is a mixture of FeSO<sub>4</sub> (PDF# 73-1057) and α-Fe<sub>2</sub>O<sub>3</sub> (PDF# 87-1165). We propose that FeS<sub>2</sub> NCs exposed

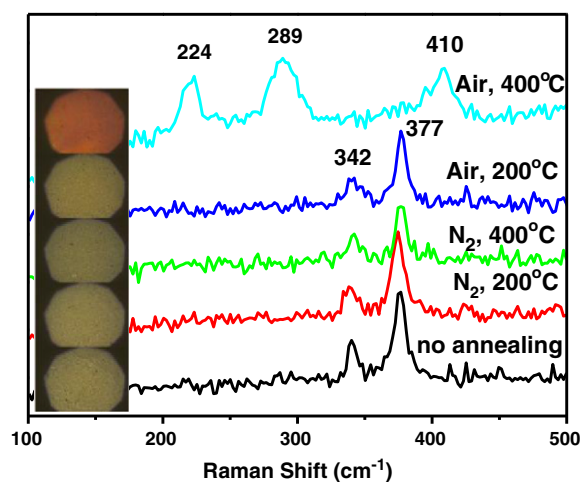
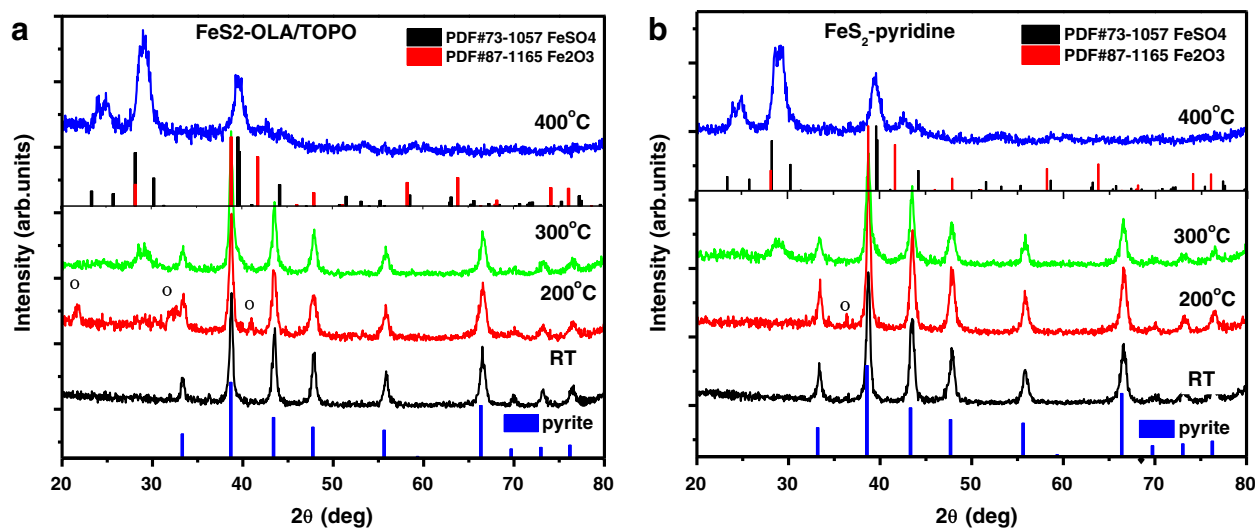
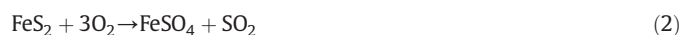


Fig. 5. Raman spectra of the FeS<sub>2</sub>-OLA/TOPO NCs after thermal annealing for 20 min at 200 and 400 °C under N<sub>2</sub> and air atmospheres (laser power of 1.5 mW). The inset shows the color change of the annealed NCs under the confocal microscope before Raman measurement.



**Fig. 6.** XRD patterns of FeS<sub>2</sub>-OLA/TOPO NCs (a) and FeS<sub>2</sub>-pyridine NCs (b) after thermal treatment in air for 20 min from room temperature (RT, 20 °C) to 400 °C. The standard XRD patterns of iron pyrite, FeSO<sub>4</sub> and hematite α-Fe<sub>2</sub>O<sub>3</sub> are given for comparison. Small peaks that are denoted by circles are possibly due to the air exposure product of the capping ligands.

to air above 300 °C underwent the reactions shown in Eqs. (2) and (3) [24,40]:



Because of the high surface-to-volume ratio in NCs, surface defects are commonly observed, such as vacancies and dangling bonds [41]. The ligands used here, OLA and TOPO, can coordinate with the surface sulfur and iron atoms with dangling bonds [5], and also act as a barrier layer against oxygen exposure. In our previous work, it was shown that TOPO capping ligands can provide enhanced long term stability against the slow but spontaneous surface decomposition to FeS and sulfur [5]. In the present work, the stability of the FeS<sub>2</sub> NCs was studied systematically upon exposing to extreme conditions, such as high light intensity, high temperature and oxygen. The ligands with long alkyl chains have demonstrated their key role in protecting the NCs from decomposition and oxidation upon laser exposure and thermal treatment. The high thermal stability of NC surfaces was observed at annealing temperatures up to 400 °C under an inert atmosphere. This may be due to the high crystallinity of the cubic FeS<sub>2</sub> NCs. After thermal annealing in air at 200 °C, both the FeS<sub>2</sub>-OLA/TOPO and FeS<sub>2</sub>-pyridine NCs did not show noticeable oxidation. This demonstrates that even in the nanoscale with large surface-to-volume ratios, the thermodynamic stability of the pyrite phase is comparable to that of the bulk pyrite materials.

#### 4. Conclusions and implications for pyrite FeS<sub>2</sub> research

The results reported here provide important guidance in designing proper pyrite FeS<sub>2</sub> NCs and the fabrication of NC films for photovoltaic applications. Of great importance is the minimization of the impact of large surface defect densities. Our results lend insight into ways to minimize the surface defects. Long-chain capping ligands such as OLA and TOPO improve long term stability against surface decomposition reactions [5] and increase thermal stability against oxidation under extreme conditions for photovoltaic applications. However these ligands are generally not preferred in PV devices due to their insulating nature. Encouragingly, small-molecule ligands such as pyridine can also preserve the surface integrity of the NCs as long as thermal annealing temperatures are below 200 °C. This high stability under medium thermal annealing temperatures provides more flexible processing options for

FeS<sub>2</sub> thin films and the practical possibility of controllable oxygen doping as a way to increase the bandgap [38].

The surface stability of iron pyrite is also a critical issue for its other versatile applications in renewable energy production and storage. As an earth abundant and nontoxic mineral, FeS<sub>2</sub> has been used as raw materials to produce sulfuric acid, catalysts in coal liquefaction [42], cathode materials for high energy density thermal batteries [43], and active layers in photoelectrochemical devices [2]. In addition, surface chemistry of iron sulfides has also played key roles in the global biogeochemical sulfur cycle and the evolution of the Earth [44,45]. Natural mines containing FeS<sub>2</sub> exposed to air and water can form acid mine drainage that has adverse environmental impacts and disrupt delicate equilibria in ecosystems [46]. Tremendous effort has been made to understand the surface physics and chemistry of iron pyrite that is in contact with air and water. This study of the pyrite surface reactivity should provide invaluable instructive information for reducing acid mine drainage, promoting mineral beneficiation, and understanding the prebiotic iron-sulfur world.

#### Acknowledgments

J.H. acknowledges the financial support from the Nebraska Public Power District through the Nebraska Center for Energy Sciences Research and Nebraska Research Initiative. The authors would like to thank Prof. Yongfeng Lu for Raman spectra measurement.

#### References

- [1] C. Wadia, A.P. Alivisatos, D.M. Kammen, Materials availability expands the opportunity for large-scale photovoltaics deployment, *Environ. Sci. Technol.* 43 (2009) 2072.
- [2] A. Ennaoui, S. Fiechter, C. Pettenkofer, N. Alonsovarante, K. Buker, M. Bronold, C. Hopfner, H. Tributsch, Iron disulfide for solar-energy conversion, *Sol. Energy Mater. Sol. Cells* 29 (1993) 289.
- [3] P.P. Altermatt, T. Kiesewetter, K. Ellmer, H. Tributsch, Specifying targets of future research in photovoltaic devices containing pyrite (FeS<sub>2</sub>) by numerical modelling, *Sol. Energy Mater. Sol. Cells* 71 (2002) 181.
- [4] J. Puthussery, S. Seefeld, N. Berry, M. Gibbs, M. Law, Colloidal iron pyrite (FeS<sub>2</sub>) nanocrystal inks for thin-film photovoltaics, *J. Am. Chem. Soc.* 133 (2011) 716.
- [5] Y. Bi, Y.B. Yuan, C.L. Exstrom, S.A. Darveau, J.S. Huang, Air stable, photosensitive, phase pure iron pyrite nanocrystal thin films for photovoltaic application, *Nano Lett.* 11 (2011) 4953.
- [6] L. Zhu, B. Richardson, J. Tanumihardja, Q.M. Yu, Controlling morphology and phase of pyrite FeS<sub>2</sub> hierarchical particles via the combination of structure-direction and chelating agents, *Crystengcomm* 14 (2012) 4188.
- [7] B.X. Yuan, W.L. Luan, S.T. Tu, One-step synthesis of cubic FeS<sub>2</sub> and flower-like FeS<sub>2</sub> particles by a solvothermal reduction process, *Dalton Trans.* 41 (2012) 772.

- [8] H.A. Macpherson, C.R. Stoldt, Iron pyrite nanocubes: size and shape considerations for photovoltaic application, *ACS Nano* 6 (2012) 8940.
- [9] M. Akhtar, J. Akhter, M.A. Malik, P. O'Brien, F. Tuna, J. Raftery, M. Helliwell, Deposition of iron sulfide nanocrystals from single source precursors, *J. Mater. Chem.* 21 (2011) 9737.
- [10] Y.J. Zhang, Y.P. Du, H.R. Xu, Q.B. Wang, Diverse-shaped iron sulfide nanostructures synthesized from a single source precursor approach, *Crystengcomm* 12 (2010) 3658.
- [11] B. Mao, Q. Dong, Z. Xiao, C.L. Exstrom, S.A. Darveau, T.E. Webber, B.D. Lund, H. Huang, Z. Kang, J. Huang, Zinc alloyed iron pyrite ternary nanocrystals for band gap broadening, *J. Mater. Chem. A* 1 (2013) 12060.
- [12] A. Ennaoui, S. Fiechter, G. Smestad, H. Tributsch (Eds.), *World Renewable Energy Congress. Energy and the Environment*, Pergamon Press, Oxford, 1990, p. 458.
- [13] K. Ellmer, H. Tributsch, *Proceedings of the 12th Workshop on Quantum Solar Energy Conversion*, Wolkenstein, Sudtiroi, Italy, May 2000, p. 11.
- [14] A. Ennaoui, S. Fiechter, H. Goslowsky, H. Tributsch, Photoactive synthetic polycrystalline pyrite, *J. Electrochem. Soc.* 132 (1985) 1579.
- [15] K. Buker, N. Alonsovante, H. Tributsch, Photovoltaic output limitation of N-FeS<sub>2</sub> (Pyrite) Schottky barriers – a temperature-dependent characterization, *J. Appl. Phys.* 72 (1992) 5721.
- [16] R. Dasbach, G. Willeke, O. Blenk, Iron sulfide for photovoltaics, *MRS Bull.* 18 (1993) 56.
- [17] M. Caban-Acevedo, M.S. Faber, Y.Z. Tan, R.J. Hamers, S. Jin, Synthesis and properties of semiconducting iron pyrite (FeS<sub>2</sub>) nanowires, *Nano Lett.* 12 (2012) 1977.
- [18] D. Lichtenberger, K. Ellmer, R. Schieck, S. Fiechter, Optical, electrical and structural-properties of polycrystalline iron-pyrite (FeS<sub>2</sub>) layers deposited by reactive DC magnetron sputtering, *Appl. Surf. Sci.* 70–1 (1993) 583.
- [19] L.P. Yu, S. Lany, R. Kykyneshi, V. Jieratum, R. Ravichandran, B. Pelatt, E. Altschul, H.A. S. Platt, J.F. Wager, D.A. Keszler, A. Zunger, Iron chalcogenide photovoltaic absorbers, *Adv. Energy Mater.* 1 (2011) 748.
- [20] R. Schieck, A. Hartmann, S. Fiechter, R. Konenkamp, H. Wetzel, Electrical-properties of natural and synthetic pyrite (FeS<sub>2</sub>) crystals, *J. Mater. Res.* 5 (1990) 1567.
- [21] T. Fukui, T. Miyadai, S. Miyahara, Photoconductivity of natural pyrite (FeS<sub>2</sub>), *J. Phys. Soc. Jpn.* 31 (1971) 1277.
- [22] C. Wadia, Y. Wu, S. Gul, S.K. Volkman, J.H. Guo, A.P. Alivisatos, Surfactant-assisted hydrothermal synthesis of single phase pyrite FeS<sub>2</sub> nanocrystals, *Chem. Mater.* 21 (2009) 2568.
- [23] S. Seefeld, M. Limpinsel, Y. Liu, N. Farhi, A. Weber, Y.N. Zhang, N. Berry, Y.J. Kwon, C.L. Perkins, J.C. Hemminger, R.Q. Wu, M. Law, Iron pyrite thin films synthesized from an Fe(acac)<sub>3</sub> ink, *J. Am. Chem. Soc.* 135 (2013) 4412.
- [24] R. Murphy, D.R. Strongin, Surface reactivity of pyrite and related sulfides, *Surf. Sci. Rep.* 64 (2009) 1.
- [25] N. Wu, R.F. Sabirianov, C.-G. Duan, W.N. Mei, D. Wisbey, Y.B. Losovyj, M. Manno, C. Leighton, E. Cai, J. Zhang, P.A. Dowben, The surface stability of CoS<sub>2</sub>(100), *J. Phys. Condens. Matter* 20 (2008) 215231.
- [26] Z.X. Yu, M.A.V. Hove, S.Y. Tong, D. Wisbey, Y.B. Losovyj, N. Wu, M. Manno, L. Wang, C. Leighton, W.N. Mei, P.A. Dowben, The structure of the CoS<sub>2</sub>(100)-(1 × 1) surface, *J. Phys. Condens. Matter* 19 (2007) 249001.
- [27] A.M.A. El Halim, S. Fiechter, H. Tributsch, Control of interfacial barriers in n-type FeS<sub>2</sub> (pyrite) by electrodepositing metals (Co, Cu) forming isostructural disulfides, *Electrochim. Acta* 47 (2002) 2615.
- [28] M. Caban-Acevedo, D. Liang, K.S. Chew, J.P. DeGrave, N.S. Kaiser, S. Jin, Synthesis, characterization, and variable range hopping transport of pyrite (FeS<sub>2</sub>) nanorods, nanobelts, and nanoplates, *ACS Nano* 7 (2013) 1731.
- [29] W. Li, M. Doblinger, A. Vaneski, A.L. Rogach, F. Jackel, J. Feldmann, Pyrite nanocrystals: shape-controlled synthesis and tunable optical properties via reversible self-assembly, *J. Mater. Chem.* 21 (2011) 17946.
- [30] J.M. Lucas, C.-C. Tuan, S.D. Lounis, D.K. Britt, R. Qiao, W. Yang, A. Lanzara, A.P. Alivisatos, Ligand-controlled colloidal synthesis and electronic structure characterization of cubic iron pyrite (FeS<sub>2</sub>) nanocrystals, *Chem. Mater.* 25 (2013) 1615.
- [31] W. Li, T. Dittrich, F. Jäckel, J. Feldmann, Optical and electronic properties of pyrite nanocrystal thin films: the role of ligands, *Small* 10 (2014) 1194.
- [32] D.Y. Wang, Y.T. Jiang, C.C. Lin, S.S. Li, Y.T. Wang, C.C. Chen, C.W. Chen, Solution-processable pyrite FeS<sub>2</sub> nanocrystals for the fabrication of heterojunction photodiodes with visible to NIR photodetection, *Adv. Mater.* 24 (2012) 3415.
- [33] M.Y.C. Teo, S.A. Kulinich, O.A. Plaksin, A.L. Zhu, Photoinduced structural conversions of transition metal chalcogenide materials, *J. Phys. Chem. A* 114 (2010) 4173.
- [34] N. Shukla, C. Liu, P.M. Jones, D. Weller, FTIR study of surfactant bonding to FePt nanoparticles, *J. Magn. Magn. Mater.* 266 (2003) 178.
- [35] J.A. Bourdoiseau, M. Jeannin, R. Sabot, C. Remazeilles, P. Refait, Characterisation of mackinawite by Raman spectroscopy: effects of crystallisation, drying and oxidation, *Corros. Sci.* 50 (2008) 3247.
- [36] E.B. Hansson, M.S. Odziemkowski, R.W. Gillham, Formation of poorly crystalline iron monosulfides: surface redox reactions on high purity iron, *Spectroelectrochemical studies*, *Corros. Sci.* 48 (2006) 3767.
- [37] A. Boughriet, R.S. Figueiredo, J. Laureyns, P. Recourt, Identification of newly generated iron phases in recent anoxic sediments: Fe-57 Mossbauer and microRaman spectroscopic studies, *J. Chem. Soc. Faraday Trans.* 93 (1997) 3209.
- [38] J. Hu, Y.N. Zhang, M. Law, R.Q. Wu, Increasing the band gap of iron pyrite by alloying with oxygen, *J. Am. Chem. Soc.* 134 (2012) 13216.
- [39] D.L.A. deFaria, S.V. Silva, M.T. deOliveira, Raman microspectroscopy of some iron oxides and oxyhydroxides, *J. Raman Spectrosc.* 28 (1997) 873.
- [40] C.M. Eggleston, J.J. Ehrhardt, W. Stumm, Surface structural controls on pyrite oxidation kinetics: an XPS-UPS, STM, and modeling study, *Am. Mineral.* 81 (1996) 1036.
- [41] C. Burda, X.B. Chen, R. Narayanan, M.A. El-Sayed, Chemistry and properties of nanocrystals of different shapes, *Chem. Rev.* 105 (2005) 1025.
- [42] R.M. Baldwin, S. Vinciguerra, Coal-liquefaction catalysis – iron pyrite and hydrogen-sulfide, *Fuel* 62 (1983) 498.
- [43] P.J. Masset, R.A. Guidotti, Thermal activated (“thermal”) battery technology – part III: FeS(2) cathode material, *J. Power Sources* 177 (2008) 595.
- [44] D. Rickard, G.W. Luther, Chemistry of iron sulfides, *Chem. Rev.* 107 (2007) 514.
- [45] D. Rickard, M.A.A. Schoonen, G.W. Luther, Chemistry of iron sulfides in sedimentary environments, *Geochem. Transform. Sediment. Sulfur* 612 (1995) 168.
- [46] D.B. Johnson, K.B. Hallberg, Acid mine drainage remediation options: a review, *Sci. Total Environ.* 338 (2005) 3.